Multiline, superbroadband and sun-color oscillation of a LiF:F_2^- color-center laser

Tasoltan T. Basiev, Petr G. Zverev, Vladimir V. Fedorov, and Sergey B. Mirov

We report experimental and theoretical studies of the temporal, spectral, and spatial features of a superbroadband laser. The results obtained show that the superbroadband room-temperature operable LiF:F_2^- color-center laser can provide low-coherence, high-intensity laser radiation with a spectral width of 1400 A centered at 1.14 μm and 700 A in the visible range from green to red and exhibit good spatial collimation with a divergence of between 5 and 6 mrad. Oscillation of all the lines of a superbroadband spectrum is completely synchronous and occurs almost simultaneously with the pump pulse, exhibiting 4–9-ns pulse delay at 20-ns pump pulse duration. Second-harmonic generation of superbroadband oscillation spectrum was realized with an overall efficiency of 10%.

Key words: Superbroadband laser, color-center laser, second-harmonic generation, divergence, multifrequency oscillation, fluorescence.

1. Introduction

Our recently developed superbroadband solid-state laser (SSSL) with a LiF:F_2^- color-center active element was reported to provide two types of laser radiation: simultaneous superbroadband laser radiation in the 1.1–1.25-μm spectral region and multifrequency or spectrally controlled laser oscillation.[1–4] By simultaneous second-harmonic generation (SHG) in one nonlinear crystal, oscillation in the visible spectral range from 0.55 to 0.62 μm was obtained in both regimes. We call it a sun-color laser. The superbroadband laser oscillation can be applied to fast fluorescence and absorption spectroscopy, two-photon nonlinear spectroscopy, nanosecond color photography, optical communication systems, information coding, and other scientific and technical areas.

Another possible application of the SSSL is based on its unique possibility to provide oscillation on different spectral lines or in the wide spectral region simultaneously, with almost no temporal delay. The spatial mixture of this light can be called a pulse of low-coherence light, that is, a pulse of radiation with a wide, smooth spectral distribution whose spectral lines travel simultaneously in time along the same direction. Low-coherence sources based on light-emitting diodes have found applications in medical optical tomography[5,6] as well as in interferometry for invasive measurements of silicon wafers and sheet growth monitoring.[7,8] The SSSL has a much higher output average and peak intensity than diodes, as well as a spectral range that is ten times wider.

In this paper we discuss the temporal, spectral, and spatial features of SSSL oscillation in IR and visible (sun-color) radiation. The analysis of simultaneous SHG in different nonlinear crystals is presented. Some aspects of collimating and spatial mixing of SSSL output radiation are discussed. The mixing of SSSL output allows us to receive a low-coherence laser light with a spectral width as high as 1400 A in the IR spectral region and 700 A in the visible spectral range.

2. Principles of Superbroadband Laser Operation

Recently demonstrated new regimes of lasing[1–4]—superbroadband or multifrequency generation of color-center lasers with a spectral width practically coinciding with the luminescence spectrum of the color-center crystal (CCC)—were realized because of the new laser cavity construction shown in Fig. 1. The laser operates as follows:

An active medium (AM) is longitudinally or quasi-longitudinally pumped through the input end dichroic mirror (M_1) by pulsed neodymium laser

T. T. Basiev, P. G. Zverev, and V. V. Fedorov are with the General Physics Institute, Vavilov Street 38, Moscow 117942, Russia. S. B. Mirov is with the Department of Physics, University of Alabama at Birmingham, Birmingham, Alabama 35294-1170.

Received 22 July 1996; revised manuscript received 4 October 1996.

0003-6935/97/122515-08$10.00/0

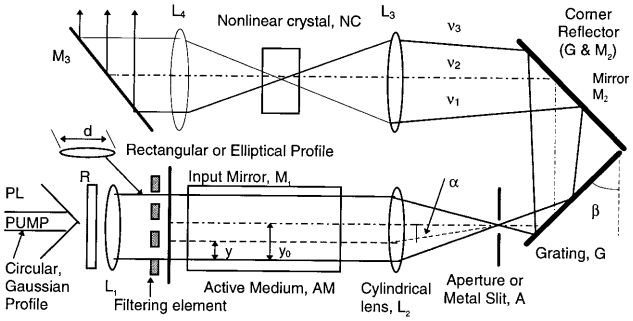

Fig. 1. Solid-state laser with superbroadband or control generation spectrum optical setup.

radiation, having an elliptical spatial profile that is formed by a reshaping–focusing system (R L_1). Emission from the whole pumped volume of the active medium passes through the focusing element (L_2) into the off-axis mode suppression element (A), which separates only a part of it from the amplified emission that is spread parallel to the resonator axis. This separated radiation is diffracted on the grating (G). The grating works as an output coupler in the autocollimating regime in first-order diffraction and returns radiation back to the suppression element (A). The off-axis mode suppression element, in its turn, extracts from the diffracted radiation only the radiation of the main laser modes parallel to the laser optical axis and secondary laser modes that diverge from the optical axes are expelled from the generation process. The radiation of the main laser modes, each with a distinct wavelength, is collimated by the focusing element (L_2) and directed back to the active medium. Each mode with its distinct wavelength has its own trajectory. This radiation, along with the stimulated radiation provoked by it, is reflected directly back by the end mirror (M_1). This process gives rise to the superbroadband multifrequency oscillation—independent oscillation of different parts of the active medium with different wavelengths, covering practically the whole spectral region of the active medium amplification band. This results in each part of the crystal parallel to the laser axis working as an independent laser with its own wavelength lying within the broad AM luminescence spectrum. We refer to it as a narrow line laser. Its oscillation wavelength is determined by the equation for diffraction grating working in the autocollimation regime as

$$\lambda = 2d \sin \theta, \tag{1}$$

where d is the grating spacing and θ is the incident angle. The diffraction grating also works as an output coupler, so that zero-order diffraction is extracted out of the cavity. The corner reflector mirror is used to turn the output radiation to make a more compact laser design. Thus, the SSSL overall output radiation has a spatially spread rainbow spectra divergent in the horizontal plane, so that each narrow line laser has its own angular direction in the output radiation.

3. Temporal behavior of Superbroadband Solid-State Laser radiation

The important feature of the nanosecond SSSL output radiation is a simultaneous oscillation of the radiation with different wavelengths. The LiF:F_2^- CCC is known to be an active medium with a high-gain coefficient. Because of a high fluorescence cross section and gain, the efficient tunable oscillation of a LiF:F_2^- laser can be obtained with a high transmission output coupler. Typical values of the optimal output coupler are between approximately 20 and 40%.[1] This results in the fact that several passes around the cavity are required for developing laser oscillation. In its turn this gives a small temporal delay between the pump and the oscillating pulses.

Let us consider the temporal behavior of the oscillations of narrow line lasers in a LiF:F_2^- SSSL. We analyze the approximate analytical equations that relate to the time delay between the pump and the oscillating pulses, spectroscopic properties of the active medium, parameters of the laser cavity and intensity of the pulsed pump radiation, and compare theoretical approximation with the experimental results.

Disregarding the details, the LiF:F_2^- color-center laser can be considered as a four-level system. The pump radiation is absorbed in the wide band of the electric-dipole electron-vibration transition $1 \Rightarrow 2^*$. In a period of time of the order of 10^{-12}–10^{-13} s, nonradiative relaxation to the minimum of the potential curve of the excited electronic state $2^* \Rightarrow 2$ occurs, accompanied by phonon emission. Then a radiative electron-vibration transition of $2 \Rightarrow 1^*$ occurs with a lifetime of 68 ns.[9] Within the framework of the described model and conventional rate equations for the electronic level population density, it is easy to obtain the following differential equations for the population density of excited centers N_2 and oscillating photon flux density I_g:

$$\frac{\partial N_2}{\partial t} = -\{[\sigma_{21}(\nu_g) + \sigma_{12}(\nu_g)]I_g + [\sigma_{21}(\nu_p) + \sigma_{12}(\nu_p)]I_p + \tau_2^{-1}\}N_2 + [\sigma_{12}(\nu_p)I_p + \sigma_{12}(\nu_g)I_g]N, \tag{2}$$

$$\frac{\partial I_g}{\partial t} = t_{\text{cav}}^{-1} I_g\{2lN_2[\sigma_{21}(\nu_g) + \sigma_{12}(\nu_g)] - 2lN\sigma_{12}(\nu_g) + 2L[\beta_{\text{active}} + \beta_{\text{passive}}]\}. \tag{3}$$

Here $\sigma_{12}(\nu_p)$ and $\sigma_{12}(\nu_g)$ are the cross sections of the excitation of optical centers at pumping (ν_p) and generation (ν_g) frequencies, respectively; $\sigma_{21}(\nu_p)$ and $\sigma_{21}(\nu_g)$ are the corresponding cross sections of stimulated emission to a lower level for the above frequencies; I_p and I_g are the flux densities of pump and generating photons; τ_2^{-1} is the probability of spontaneous relaxation of the upper laser level, and N is the total number of F_2^- color centers in 1 cm^3 of a LiF crystal. In Eq. (3) t_{cav}^{-1} corresponds to the cavity round-trip time, l and L are the active media and cavity lengths, respectively; and $\beta_{\text{active}} = (2\text{L})^{-1} \ln(R)$

and $\beta_{passive}$ are the active and passive cavity losses in the laser cavity, for which R is the output coupler reflectivity. The cavity passive losses include the passive losses inside an active element, diffraction losses, parasitic absorption, and scattering in the optical elements, including diffraction grating.

As the spontaneous relaxation time of F_2^- color centers (τ_2) at room temperature is 68 ns, which is much higher than the duration of pump and oscillating pulses (10–30 ns) that we used in our experiments, the spontaneous relaxation term $(\tau_2)^{-1}$ in Eq. (2) can be neglected.

One of the features of the nanosecond pulsed pump is its high radiation intensity I_p that is much higher than the corresponding saturation intensity of the $1 \Rightarrow 2$ transition for F_2^- that was measured to be 0.14 MW/cm^2.[10,11] So the oscillation of a LiF:F_2^- color-center laser under nanosecond pulsed pumping can be considered as a consequence of independent temporal stages. The first is a quick bleaching of the active medium to a saturated state, the second is a development of laser oscillation with quasi-stable population inversion, and the third is a saturation of the oscillation. It is known that the delay time of the oscillation with respect to the pump pulse is determined by the first two stages. We now consider the time duration of these processes. For simplicity, a uniform pulse excitation with pump photon flux density of I_p and a duration t_p is considered. During the first stage the photon flux at oscillating frequency I_g is negligible. The saturation of the active media can be obtained when $dN_2/dt = 0$ and the saturated state population of excited state N_2 can be determined from Eq. (2) as follows:

$$N_2^{(\mathrm{sat})} = \frac{N\sigma_{12}(\nu_p)}{\sigma_{21}(\nu_p) + \sigma_{12}(\nu_p)}. \tag{4}$$

The time duration of this stage t_1 can be obtained if we calculate the energy that is necessary to excite $N_2^{(\mathrm{sat})}$ number of color centers:

$$t_1 = \frac{N_2^{(\mathrm{sat})} lS}{I_p S} = \frac{Nl\sigma_{12}(\nu_p)}{I_p[\sigma_{21}(\nu_p) + \sigma_{12}(\nu_p)]}. \tag{5}$$

Here $Nl\sigma_{12}(\nu_p)$ is equal to the initial or low-field optical density of the active medium at the pump wavelength.

The second temporal stage of the oscillation can be considered as amplification at the generation wavelength from the initial photon flux density level $I_g^{(0)}$ to the value when the probability of stimulated transitions under oscillation radiation becomes comparable with the probability of the pump absorption. The oscillation of this stage is described by Eq. (3), assuming that $N_2 = N_2^{(\mathrm{sat})} = \mathrm{const}$. Thus, one can obtain the following:

$$I_g = I_g^{(0)}[R\Gamma_{\mathrm{pass}}K^2(\nu_g)]^{t_2/t_{\mathrm{cavity}}}. \tag{6}$$

Here t_2/t_{cavity} is an effective number of round trips through the cavity, Γ_{pass} represents the cavity passive losses $\Gamma_{\mathrm{pass}} = \exp(2L\ \beta_{\mathrm{passive}})$, and $K(\nu_g)$ is a one-pass unsaturated gain coefficient in the active medium at oscillating frequency ν_g, defined as

$$K(\nu_g) = \exp\{[\sigma_{21}(\nu_g) + \sigma_{12}(\nu_g)]N_2^{(\mathrm{sat})}l - \sigma_{12}(\nu_g)Nl\}. \tag{7}$$

The laser generation build-up time for the second stage t_2 can be found from Eqs. (5)–(7) as

$$t_2 = t_{\mathrm{cavity}} \frac{\ln[I_g/I_g^{(o)}]}{2Nl\,\dfrac{\sigma_{12}(\nu_p)\sigma_{21}(\nu_g) - \sigma_{21}(\nu_p)\sigma_{12}(\nu_g)}{\sigma_{12}(\nu_p) + \sigma_{21}(\nu_p)} + \ln R + 2L\beta_{\mathrm{passive}}}. \tag{8}$$

The total delay time can be obtained as a sum of the delay times of the first and second stages: $t_{\mathrm{delay}} = t_1 + t_2$.

For the LiF:F_2^- four-level system, with a Gaussian luminescence band of the full width at half-maximum of $\Delta\nu = 4.13 \times 10^{13}$ Hz,[1] the cross section of stimulated emission ($\sigma_e^{\,o}$) at the luminescence band peak λ_o can be calculated from the following well-known formula[9]:

$$\sigma_e^{\,o} = 2\sqrt{\frac{\ln 2}{\pi}}\,\frac{\lambda_o^{\,2}}{8\pi n_r^{\,2}\Delta\nu}\,\frac{\eta}{\tau_2}, \tag{9}$$

where $n_r = 1.39$ is the refractive index of a LiF crystal, $\eta = 0.8$ and $\tau_2 = 68$ ns are, respectively, the quantum efficiency and fluorescence lifetime of a LiF:F_2^- crystal measured at room temperature.[1] So, the value of $\sigma_e^{\,o}$ is 7.5×10^{-17} cm^2.

The cross section of stimulated absorption σ_a of F_2^- centers at the pump wavelength $\lambda_p = 1064$ nm is equal to 2×10^{-17} cm^2.[10,11] The total density of the F_2^- centers in the LiF crystal, featuring a typical absorption coefficient for F_2^- active elements at $\lambda = 1064$ nm, $k = 0.6$ cm^{-1}, can be defined as $N = k/\sigma_a = 3 \times 10^{16}$ cm^{-3}.

To calculate the temporal delays for the maximum oscillation wavelength (1.14 μm) values we need to substitute the characteristic data for our experimental setup. These were $I_p = 1 \times 10^{26}$ photon/s cm^2 (20 MW/cm^2); 30% reflectivity of the output coupler; $l = 40$ mm and $L = 15$ cm, respectively, for the lengths of the active element and cavity; and the term $[\sigma_{12}(\nu_p)\sigma_{21}(\nu_g) - \sigma_{21}(\nu_p)\sigma_{12}(\nu_g)][\sigma_{12}(\nu_p) + \sigma_{21}(\nu_p)]^{-1}$ equals 1.9×10^{-17} cm^2 for a 1.14-μm oscillating wavelength.[11] The time delay that is due to the first stage equals $t_1^{(1.14)} = 0.33$ ns.

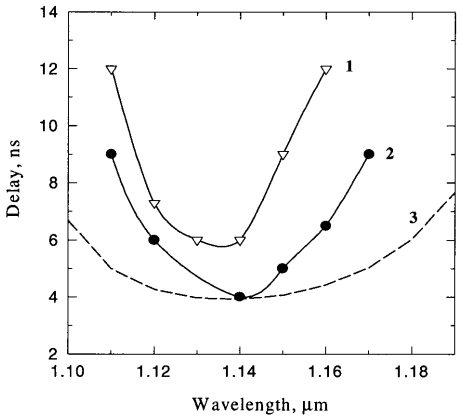

Fig. 2. Experimental (curves 1 and 2) and theoretical (dashed curve 3) dependencies of the time delay of different wavelength component oscillations in the SSSL output radiation with respect to the pump pulse for two pump energies 25 (curve 1) and 14 mJ (curve 2).

To investigate the temporal behavior of the SSSL output we measured a time delay of the oscillation at a certain wavelength. Figure 2 shows the experimental relative pulse delay dependencies for pumping energies of 25 and 14 mJ (pump intensities of 20 and 11 MW/cm^2, respectively). One can see that the experimental data for temporal delays for different wavelength components of a SSSL in the center of the spectral range are small and increase at the edges to between approximately 4 and 9 ns for a high pumping energy (25 mJ) and between 6 and 12 ns for a lower energy (14 mJ).

Using the dependence for $\sigma_e(\nu)$ as

$$\sigma_e(\nu) = \sigma_e{}^o \exp\left[-4 \ln 2 \frac{(\nu - \nu_o)^2}{(\Delta\nu)^2}\right] \qquad (10)$$

and Eq. (8), one can estimate the dependence $t_2 = f(\lambda)$ (see dashed curve in Fig. 2). From Fig. 2 it is clear that the simple laser model described above fits qualitatively well the dynamics of laser oscillation in a SSSL. In our calculation we used $\ln[I_g/I_g{}^{(0)}] = 18.4$ and $\Gamma_{\text{pass}} = 0.7$. Higher curvature of the experimental dependence with respect to the theoretical one can be explained by the dependence of $\ln[I_g/I_g{}^{(0)}]$ on the oscillation frequency and pump density because of the influence of two-pass superluminescence in a high-gain LiF:$F_2{}^-$ active medium on the initial photon flux value $[I_g{}^{(0)}]$. Another reason relates to the nonuniform distribution of the pumping energy in the experiment. A quasi-circular Gaussian pump beam was reshaped to an elliptical nonuniform profile by means of a cylindrical lens. It exhibits maximum intensity in the center of the beam (corresponding to the emission band peak) and features a continuous drop of intensity at the peripheral areas (corresponding to the short and long wavelengths of the emission bands). This results in a reduction of the pump intensity at the edges of the oscillating spectra and subsequent increase of delay time. It is necessary to note that, in all the above measurements, the time delay for SSSL output was much less than the pump pulse duration and the center of the tuning band was approximately an order of magnitude less.

4. Second-harmonic generation of Superbroadband Solid-State Laser radiation

To obtain SHG of superbroadband radiation in a single nonlinear crystal, it is necessary to satisfy two requirements. The first is the phase-matching conditions for all oscillating wavelengths. The second is to provide high radiation intensity inside a nonlinear medium that would be sufficient to obtain high conversion efficiency.

The possibility of obtaining SHG of broadband laser radiation with a spectral width of as much as 100 A using the compensation of phase-matching angular dispersion in a nonlinear crystal with angular dispersion after the grating was demonstrated in a number of papers.[12,13] In a SSSL the simultaneous SHG must be realized for superbroadband radiation with a spectral width that is greater than ten times wider—as much as 1500 A.

The angular distribution of oscillating wavelengths in SSSL output radiation after the grating is described by Eq. (1). If we consider that laser oscillation with 1.14-μm radiation wavelength travels along the laser axis, the angular distribution of different oscillation wavelengths is as follows:

$$\alpha(\lambda) = \arcsin(\lambda_{1.14}/2d) - \arcsin(\lambda/2d). \qquad (11)$$

The collimation of the SSSL output with a standard spherical lens changes the slope of the angular dependence with respect to the lens focal length and its position. Its angular magnification can be written using a standard lens formula such as

$$M = \tan \alpha_{\text{out}}/\tan \alpha_{\text{in}} = a/b = (a - F)/F, \qquad (12)$$

where α_{out} and α_{in} are, respectively, the angles of refracted and incident beams; a and b are the object and image distances; and F is the focal length of the lens. Thus, the total angular-wavelength distribution of collimated SSSL IR output can be described as follows:

$$\alpha(\lambda) = \arctan\left\{\frac{(a - F)}{F} \tan[\arcsin(\lambda_{1.14}/2d) - \arcsin(\lambda/2d)]\right\}. \qquad (13)$$

To obtain simultaneous SHG of the SSSL output with such angular-wavelength distribution, it is necessary to derive the wavelength dependencies of phase-matching angles for different nonlinear crystals. Lithium niobate, KDP, lithium iodate, BBO, KTP, and Banana nonlinear crystals were considered in our analysis. The expressions for the phase-matching angles and refractive indices of the above crystals can be written according to Ref. 14. The types of phase-matching condition can be divided into two main groups: (1) *ooe* or *eeo* and (2) *oeo* or *oee*.

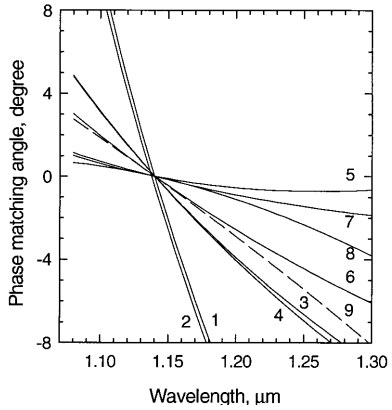

Fig. 3. Wavelength dependencies of phase-matching angles for SHG outside nonlinear media for $LiNbO_3$ (curve 1), Banana (curve 2), KTP (curves 3 and 4), LBO (curve 5), $LiIO_3$ (curve 6), BBO (curve 7), and KDP (curve 8) crystals. All the crystals are cut for 1.14 μm. Dashed curve 9 corresponds to the angular-wavelength distribution of SSSL output in the near IR.

As the IR output of a SSSL has angular distribution and enters the nonlinear crystal under different incident angles, for the second group, the angles for *o* and *e* IR interacting beams inside the nonlinear crystal will be different. This means that only the first type of phase-matching conditions can result in the simultaneous SHG of SSSL output radiation and thus is considered in our analysis.

The calculated wavelength dependencies of phase-matching angles outside the SHG crystal for different nonlinear media are shown in Fig. 3. The SHG crystals were considered to be cut for the central wavelength of the oscillation spectra, that is, 1.14 μm. The results on the slope and averaged curvature calculations are shown in Table 1. One can see that $LiNbO_3$ (curve 1 in Fig. 3) and Banana (curve 2 in Fig. 3) crystals have very strong angular dependencies in the 1.08–1.25-μm spectral region and can hardly be used for SHG for SSSL. The dependence for $LiIO_3$ crystal (curve 6 in Fig. 3) has the same slope as that for IR output of SSSL, whereas its curvature is slightly different. To use KTP crystals for SHG, it is necessary to install a collimator with angular magnification of approximately 1.6. This also results in a corresponding increase of the curvature of the output radiation dependence and higher discrepancy of the angular dependencies at the edges of the oscillation spectral range.

BBO and KDP crystals are also promising for obtaining simultaneous SHG of SSSL output. For these crystals it is necessary to collimate the IR output with magnifications of 0.28 and 0.3, respectively. This results in an increase of the image distance and size of the beam spot. The drawback of KDP crystal is its small nonlinearity and correspondingly low conversion efficiency.

For our testing experiments a $LiIO_3$ crystal was chosen as it has the same slope of angular dependence and there is no need for any angular magnification in the collimator. At the same time it has a high nonlinear coefficient that is 12 times higher than that for KDP and three times higher than that for BBO. A 15-mm-long $LiIO_3$ crystal with a collimating lens having a 70-mm focal length placed 140 mm away from intracavity aperture A provided no angular magnification to obtain the best fit of the angular distribution of the IR SSSL output and phase matching with SHG visible radiation in a nonlinear crystal. The highest conversion efficiency was obtained when the SHG crystal was placed in the focal position of the vertical plane. Spherical focusing of a divergent elliptical SSSL infrared output radiation into a SHG crystal results in rainbow elliptical visible radiation.

The results of obtaining simultaneous SHG in a $LiJO_3$ nonlinear crystal of record wide superbroadband spectra of continuous spectral distribution without a sharp reduction are presented in Figs. 4–6. Because of different second derivatives there is some deviation in the angular dependencies between the dependence for $LiIO_3$ crystal and that for the diffraction grating. This results in the SHG of only 80% of the superbroadband oscillation spectra with an overall efficiency of 10%. It is worth mentioning that

Table 1. Slope and Curvature at 1.14-μm Wavelength of the SHG Phase-Matching Angle Dependence Versus Wavelength in Some Nonlinear SHG Crystals

Curve Number	Crystal	Angle with Respect to the *C* Axis	Type of Phase Matching	Slope at 1.14 mm ($\times 10^{-2}$ nm^{-1})	Curvature at 1.14 μm ($\times 10^{-4}$ nm^{-2})
1	$LiNbO_3$	64.45	*ooe*	22	12.25
2	Banana	65.96	*ooe Y–Z* plane	21.7	10.08
3	KTP	45.51	*eeo X–Z* plane ($\theta < Vz$)	7.3	2.43
4	KTP	35.77	*eeo Y–Z* plane	7.4	2.18
5	LBO	33.13	*ooe X–Z* plane ($\theta < Vz$)	1.3	1.23
6	LiIO3	27.89	*ooe*	4.7	1.19
7	BBO	21.8	*ooe*	1.7	0.72
8	KDP	41.72	*ooe*	1.46	1.22
9	Diffraction grating			4.7	−0.37

Fig. 4. Image of the SHG of LiF:F_2^- SSSL 4.3 m away from the SHG crystal in a multifrequency operation without collimation.

developing a collimator with special correction of its surface shapes can result in a complete overlap of the angular-wavelength dependencies and can increase the total SHG efficiency to the typical values of SHG for a narrow line laser oscillation.

5. Divergence of Superbroadband Solid-State Laser Output Radiation

As was shown above the infrared output radiation of a LiF:F_2^- SSSL has high rainbow divergence in the horizontal plane determined by Eq. (1). In the absence of any collimating optics, its divergence is approximately 10 deg for the whole oscillation spectra from 1.09 to 1.25 μm. But the divergence of each narrow line laser is low and can be determined by the laser mode structure. Previously it was shown that it is possible to obtain single transverse mode operation using an appropriately sized aperture.[4] The divergence measured in such a case was low and it was found to be between 0.4 and 1 mrad in the horizontal

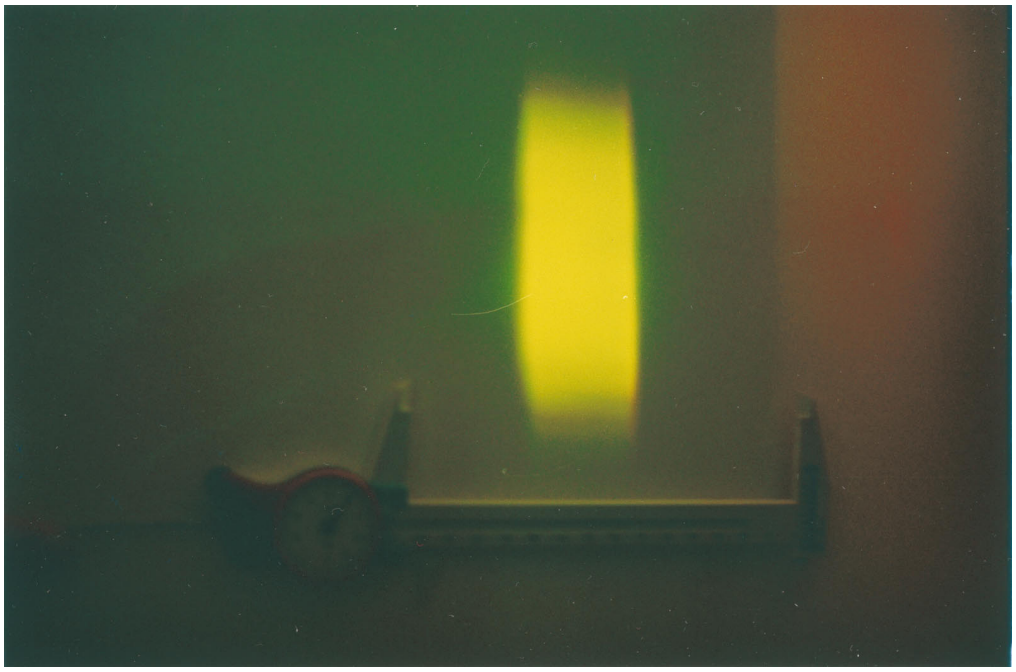

Fig. 5. Image of the SHG of LiF:F_2^- SSSL 4.3 m away from the SHG crystal in a superbroadband operation with horizontal collimation.

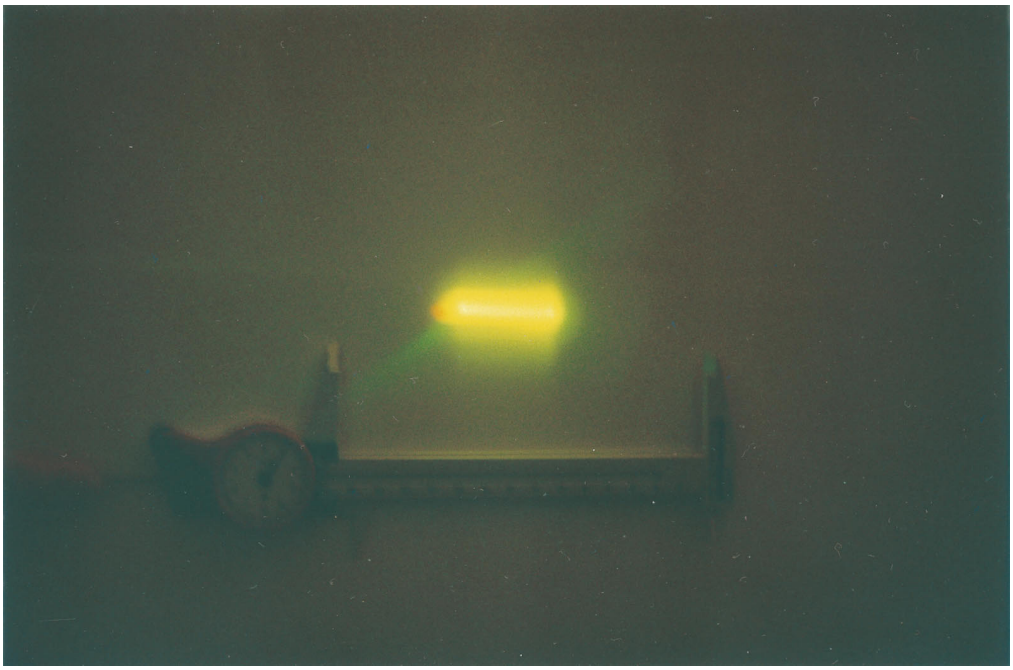

Fig. 6. Image of the SHG of LiF:F_2^- SSSL 4.3 m away from the SHG crystal in a superbroadband operation with both horizontal and vertical collimation.

plane and 3 mrad in the vertical plane. The same values for divergence were obtained for visible and IR output radiation. Without any collimation, the image of the second harmonic output, 4.3 m away from the laser, resembled a strip 38 mm high and 305 mm wide with the wavelength distribution continuously changing from red to yellow and finally to green. This corresponds to divergences of 9 and 71 mrad in the vertical and horizontal planes, respectively. The installation of a net aperture in front of the input mirror allows for switching a continuous wavelength distribution in the SSSL output to the multifrequency regime of operation. The sizes of the spots with different wavelengths at a screen 4.3 m away from the nonlinear crystal were also 38 mm in the vertical plane and vary from 21 to 28 mm with respect to its wavelength (21 mm at the red edge and 28 mm for the green) for eight wavelength oscillations (see Fig. 4). The size of complete multifrequency spectra corresponded to the size of continuous superbroadband spectra and was equal to 305 mm.

Differences in the divergence of the visible SSSL output in the two planes require the use of different collimating optics. The use of a cylindrical lens with $f = 100$ mm located 100 mm from the SHG crystal allows for seven times reduction of the divergence of the output radiation in the vertical plane, yielding a value of approximately 1.3 mrad. The horizontal collimating lens was placed at a distance $L_2 = F_2 = 260$ mm from the SHG crystal. This resulted in a 7.5 times reduction of the image size in the horizontal plane, whereas the divergence became less than 9 mrad. In this case the multicolor rainbow feature of the strip vanished and the image color became similar to bright sunlight (see Fig. 5), which is why we call our laser a sun-color laser. The horizontal divergence of the separate components in the collimated multifrequency SSSL output was found to be 5–6 mrad. Thus, the total divergence of the multiline sun-color SSSL was higher than it is for its separate components, but, in this case, it was possible to realize good spatial overlap of the various wavelength components in a single spot. The result of the best collimation of SSSL output in both planes is shown in Fig. 6.

Finally, it is necessary to note that the results that we obtained were not restricted by the internal features of a superbroadband laser but demonstrate the simple possibility to collimate and to obtain a different spectral distribution in SSSL output radiation and to provide various colors in it from green to red, sun-color beam, and various spatial shapes of beam cross section from single point to rectangular and linear.

6. Conclusions

The results obtained have shown that the superbroadband color-center laser can provide low-coherence radiation with characteristic laser features: high-intensity light with good collimation in time and space but spread along the frequency or wavelength axes. The temporal delay between different wavelength components was found to be less than the nanosecond laser pulse duration and to decrease with increased pump intensity. The high spatial features of SSSL output provides the possibility for collimating and focusing output radiation similar to the radiation of a conventional laser source, obtaining high frequency mixing in the focal point and obtaining low-coherence laser light with a spec-

tral width of 1400 A in the near-IR spectral region and 700 A in the visible range from green to red (sun color).

The investigation of SHG of a LiF:F_2^- SSSL simultaneously in one nonlinear crystal has shown that the promising SHG crystals are $LiIO_3$, BBO, and KDP. A complete overlap of angular-wavelength dependencies of phase-matching angles and SSSL IR output radiation can be obtained only by using a specially designed collimator, whereas the use of a standard spherical lens in the above experiments have shown good results with a $LiIO_3$ SHG crystal.

This research was partially supported by National Science Foundation grants OSR-9450570 and OSR-9550480, International Science Foundation grant MTB 300, and Ministry of Science and Technical Policy of Russian Federation within the framework of an All-Russian Scientific and Technological Program for Optics and Laser Physics.

References

1. T. T. Basiev and S. B. Mirov, *Room Temperature Tunable Color Center Lasers*, Vol. 16 of Laser Science and Technology Series (Gordon & Breach, New York, 1994), pp. 1–160.
2. T. T. Basiev, S. B. Mirov, P. G. Zverev, I. V. Kuznetsov, and R. Sh. Tedeev, "Solid state laser with superbroadband or control generation spectrum," U.S. patent 5,461,635 (24 October 1995).
3. T. T. Basiev, P. G. Zverev, and S. B. Mirov, "Superbroad-band laser on LiF color center crystal for near-infrared and visible spectral regions," in *Abstracts of the International Conference on Laser '93* (University of Munich, Munich, Germany, 1993).
4. T. T. Basiev, P. G. Zverev, S. B. Mirov, and V. V. Fedorov, "Solid state laser with superbroadband or control generation spectrum," in *Solid State Lasers and Nonlinear Crystals*, G. J. Quarles, L. Esterowitz, L. K. Cheng, and M. S. Sobey, eds., Proc. SPIE **2379,** 54–61 (1995).
5. D. Huang, E. A. Swanson, C. P. Lin, J. S. Schuman, W. G. Stinson, W. Chang, M. R. Hee, T. Flotte, K. Gregory, C. A. Puliafito, and J. G. Fujimoto, "Optical coherence tomography," Science **254,** 1178–1181 (1991).
6. G. J. Tearney, M. E. Brezinski, M. R. Hee, B. E. Bouma, J. A. Izatt, E. A. Swanson, J. F. Southern, R. R. Anderson, and J. G. Fujimoto, "Optical coherence tomography in multiply scattering tissue," in *Optical Tomography: Photon Migration, and Spectroscopy of Tissue and Model Media: Theory, Human Studies, and Instrumentation*, B. Chance and R. Alfano, eds., Proc. SPIE **2389,** 29–34 (1995).
7. C. M. Lawson and R. R. Michael, "Fiber-optic low-coherence interferometry for non-invasive silicon wafer characterization," J. Cryst. Growth **137,** 37–40 (1994).
8. C. M. Lawson and R. R. Michael, "Optical low-coherence reflectometry (OLCR) for dimensional monitoring of sheet-grown silicon," Microwave Opt. Technol. Lett. **7,** 305–307 (1994).
9. W. Gellermann, A. Muller, D. Wandt, S. Wilk, and F. Luty, "Formation, optical properties, and laser operation of F_2^- centers in LiF," J. Appl. Phys. **61,** 1297–1303 (1987).
10. Yu. L. Gusev, S. I. Marennikov, and V. P. Chebotaev, "Tunable color center lasers," Izv. Akad. Nauk SSSR, Ser. Fiz. **44,** 2018–2028 (1980) [Bull. Acad. Sci. USSR Phys. Ser. **44,** 15–23 (1980)].
11. A. Lupei, V. Florea, T. Dascalu, and V. Lupei, "Saturation process for F_2^- color centers absorption in LiF," Opt. Commun. **79,** 309–313 (1990).
12. V. D. Volosov and E. V. Goryachkina, "Compensation of phase-matching dispersion in generation nonmonochromatic radiation harmonics. I. Doubling of neodymium-glass radiation frequency under free-oscillation conditions," Sov. J. Quantum Electron. **3,** 1577–1583 (1976).
13. G. Szabo and Z. Bor, "Broadband frequency doubler for femtosecond pulses," Appl. Phys. B **50,** 51–54 (1990).
14. V. G. Dmitriev, G. G. Gurzadyan, and D. N. Nikogosyan, "Optics of nonlinear crystals," in *Handbook of Nonlinear Optical Crystals*, A. L. Schawlow, K. Shimoda, A. E. Siegman, and T. Tamir, eds., Vol. 64 of Springer Series in Optical Sciences (Springer-Verlag, Berlin, 1991), Chap. 2, pp. 3–13.